

We are IntechOpen, the world's leading publisher of Open Access books Built by scientists, for scientists

5,300

Open access books available

129,000

International authors and editors

155M

Downloads

Our authors are among the

154

Countries delivered to

TOP 1%

most cited scientists

12.2%

Contributors from top 500 universities



WEB OF SCIENCE™

Selection of our books indexed in the Book Citation Index
in Web of Science™ Core Collection (BKCI)

Interested in publishing with us?
Contact book.department@intechopen.com

Numbers displayed above are based on latest data collected.
For more information visit www.intechopen.com



Synthesis, Luminescence and Magnetic Properties of Novel $\text{Fe}_{0.5}\text{Gd}_{0.5}(\text{MoO}_4)_{1.5}:\text{Eu}^{3+}$ Micro/Nano (3D) Structures

Rajagopalan Krishnan and Jagannathan Thirumalai

Additional information is available at the end of the chapter

<http://dx.doi.org/10.5772/61323>

Abstract

The controlled synthesis of $\text{Fe}_{0.5}\text{Gd}_{0.5}(\text{MoO}_4)_{1.5}:\text{Eu}^{3+}$ microcrystals (self-aggregated 3D superstructures) using hydrothermal method by employing PVP as surfactant along with the state of the art of this field at present. By varying the reaction time, we have reported the morphology selection and the condition to derive novel nanoparticle sheathed bipyramid-like morphology. The rest of the parameters like, molar ratio between initial precursor / surfactant and temperature were kept as constant. The $\text{Fe}_{0.5}\text{Gd}_{0.5}(\text{MoO}_4)_{1.5}:\text{Eu}^{3+}$ microcrystals are found to be an excellent matrix for photoluminescence property and the Eu^{3+} ion serves as a good red emitting luminescent center. Further, room temperature (RT) magnetic properties of $\text{Fe}_{0.5}\text{Gd}_{0.5}(\text{MoO}_4)_{1.5}:\text{Eu}^{3+}$ were investigated in detail.

Keywords: Chemical synthesis, Electron diffraction, Crystal structure, Optical properties, Magnetic measurements

1. Introduction

Size- and shape-controlled synthesis of self-organized, three-dimensional (3D) micro/nano architectures are still challenging and much attracted in the recent years owing to vast scientific and technological interest in multifaceted research areas [11, 27, 14]. The growth and development of uniform, self-aggregated 3D super-structures through plane-to-plane coalition of the basic building blocks have been paid significant attention owing to their unusual physical, chemical properties [29, 3]. The development of self-organized architectures consents to find neoteric and diversified materials, causing momentous discovery that has been developed for the construction of a new class of micro/nanostructured devices [14, 15]. Self-aggregation of hierarchical architectures has proved to be a virtuous and expedient tool to control the

structure and properties for the fabrication of intricate networks [15]. The peculiar size and morphology of the self-assembled 3D networks determine the attributes of a material which are important for the manufacture of a novel category of micro/nano-structured devices for advanced engineering and sciences [29, 14, 13]. The supreme and hopeful approach to synthesize self-assembled 3D networks is to use a solution-based technique which is a simple route to regulate the physicochemical properties of materials [3]. Specifically, in the hydrothermal method, numerous versatile morphologies have been described by using surfactants or chelating agents [7, 16, 17]. The surface capping agent used in the hydrothermal synthesis method positively assures an effective way to regulate the nucleation, controlled growth, oriented aggregation mechanism, and self-organized 3D morphology [15, 4].

2. Recent research scenario

A wide variety of 3D super-structures can be synthesized by using a suitable amount of surfactant which reduces the particle–particle amalgamation by steric effects, thereby controlling the size and shape [15]. Up till now, a number of research works have been reported on controlled synthesis of 3D hierarchical architectures using hydrothermal technique, for example, bowknot-like $Y_2(WO_4)_3:Ln^{3+}$ [9], almond-like $(Na_{0.5}La_{0.5})MoO_4:RE^{3+}$ [14], monodisperse $CaMoO_4:Eu^{3+}$, M^+ ($M = Li, Na, K$) microspheres [18], micron-sized flower-like $NaCe(MoO_4)_2$ architectures [27], tetragonal bipyramid-like $(Na_{0.5}Gd_{0.5})MoO_4:Ln^{3+}$ [15], rugby-like $NaEu(MoO_4)_2$ microstructures [26], sheaf-like $Gd_2(MoO_4)_3$ [24], etc. Large-scale assert for phosphor materials as efficient sources of energy that can supply sustained proficiency is growing gradually. Current research in phosphors is focused on new materials having both luminescence and magnetic properties in a single entity based on the presence of trivalent lanthanide ions (Ln^{3+}) with magnetic Fe^{3+} ions. These bifunctional materials have attracted worldwide intense research, because their up/down conversion luminescence and para/ferromagnetic properties are strongly required for therapeutics, contrast agents in magnetic resonance (MRI), fluorescent bioimaging in biophotonics, drug delivery and lumino-magnetic applications [6, 13, 19]. The phosphor particles can be magnetically directed, aligned, tracked, after applying the external magnetic fields. Subsequently, their luminescence can be visualized under optical excitation, which can be used widely for biological labeling, imaging of human and animal cells, tissues, and in vitro, in vivo applications [22, 25].

Phosphor	Type of luminescence investigated	Observed magnetism	Reference
$Gd_2O_2S:Yb/Er$	Upconversion	Paramagnetic	[1]
$NaGdF_4:Yb^{3+}, Ln^{3+}$	Upconversion	Paramagnetic	[8]
$YAG:Ce^{3+}$	Downconversion	Ferromagnetism	[10]
$(Na_{0.5}La_{0.5})MoO_4:Eu^{3+}$	Up/down conversion	Ferromagnetism	[15]
$(Na_{0.5}Gd_{0.5})MoO_4:Eu^{3+}$	Up/down conversion	Paramagnetic	[14]

Table 1. Recent investigation of magnetic and luminescence properties of various phosphors.

The luminescence and magnetic properties of lanthanide ions doped iron-based inorganic compounds that are synthesized by different research groups are detailed as follows. The novel $\text{Fe}_3\text{O}_4@\text{YPO}_4:\text{Re}$ (Re = Tb, Eu) magnetic-fluorescent hybrid spheres were prepared using solvothermal and co-precipitation techniques [25]. The obtained nanostructures are an excellent platform to integrate fluorescent materials and magnetite into one single entity to exhibit both magnetic and fluorescent properties [25]. Wang et al. [25] reported that human cervical carcinoma Hela cells were successfully labeled by using the $\text{Fe}_3\text{O}_4@\text{YPO}_4:\text{Re}$ hybrid spheres. Zhang et al. [29] synthesized orthorhombic cubic GdFeO_3 particles by using a facile hydrothermal method. The emission color of cubic GdFeO_3 particles could be adjusted effectively by doping different lanthanide activators [29]. Also, cubic GdFeO_3 particles exhibiting paramagnetic properties are reported to be used as an excellent luminescence and magnetic material [29]. To replace the existing halide-based upconverting phosphors for infrared-based biomedical imaging [1], nontoxic $\text{Gd}_2\text{O}_2\text{S}:\text{Yb}/\text{Er}$ is synthesized using flux fusion method. The synthesized phosphor not only enables near-IR imaging features but also at the same time could be used as a contrast agent in MRI imaging [1]. Multifunctional luminescent-magnetic YAG:Ce nano-phosphors were synthesized by post-heat solidified combustion technique, post-heated hydrothermal-homogenous precipitation, and post-heated auto-clave techniques, respectively, using inexpensive aluminum and yttrium nitrates as the starting materials and urea as the homogenizing precipitant [10]. Since the yttrium and aluminium are non-magnetic elements, the origin of ferromagnetism of these nonmagnetic oxides could be attributed solely to the defects and/or oxygen vacancies [10]. The novel YAG:Ce nanophosphor exhibits the ferromagnetic behavior which finds the way for a new class of magneto-optic and spintronic materials for a wide variety of applications. The multicolor upconversion emissions and paramagnetic nature were observed in $\beta\text{-NaGdF}_4$ crystals, which were synthesized by one-step precipitation method at room temperature [8]. To control the crystal size and morphology of the $\beta\text{-NaGdF}_4$ crystals, different types of surfactants, namely Na_2EDTA , PVP, SDS, and Na_2tar , were introduced during the synthesis procedure. Due to the presence of paramagnetic Gd^{3+} ions, $\beta\text{-NaGdF}_4$ crystals exhibit paramagnetic behavior, which is a favorable bifunctional candidate for bioimaging applications [8].

Scheelite-type metal molybdates are considered as an ideal candidate, and are receiving accelerating interest due to their remarkable luminescence, magnetic, catalytic, sensing, and photocatalytic properties [13]. Scheelite-type crystalline structures, with the general chemical formula such as $(\text{Na}_{0.5}\text{R}_{0.5})\text{MoO}_4:\text{Ln}^{3+}$ [15, 14]; $\text{BaMoO}_4:\text{Ln}^{3+}$ [23]; $\text{Ca}_{0.5}\text{R}(\text{MoO}_4)_2:\text{Ln}^{3+}$ [20]; $\text{Fe}_{0.5}\text{R}_{0.5}(\text{MoO}_4)_{1.5}:\text{Ln}^{3+}$ [13] (where R = La or Gd or Y and Ln = Eu, Tb, Dy, etc.) etc., where molybdenum atoms are coordinated tetrahedrally, have recently attracted great attention because of their promising applications in the opto-electronics [14, 15]. In the crystal structure of $\text{Fe}_{0.5}\text{R}_{0.5}(\text{MoO}_4)_{1.5}:\text{Ln}^{3+}$, trivalent Fe^{3+} , $\text{R}^{3+}/\text{Ln}^{3+}$ jointly occupy the dodecahedral positions and molybdenum (Mo^{6+}) atoms populated at the center of the tetrahedral symmetry coordinated with four equivalent oxygen atoms. Scheelite-type metal molybdates with the general formula have been synthesized by various techniques, which include hydrothermal method [14, 15], solid-state reaction technique [12], hydrothermal-assisted solid-state reaction [28], and pulsed laser deposition technique [21]. The random distribution of R^{3+} (La or Gd or Y) in the scheelite tetragonal structures show an intense and broad absorption band in the near UV- region [15].

Among all these molybdates, $(\text{Fe}_{0.5}\text{Gd}_{0.5})\text{MoO}_4:\text{Eu}^{3+}$ is an important opto-magnetic material and possess good luminescence property. Due to the notable emission spectral lines in Ln^{3+} doped phosphors extending from ultraviolet to infra-red region and its magnetic properties may open up a new platform to design and formulate other inorganic functional materials with for potential magnetic and luminescence applications [13], there is a great deal of scientific and technological interest in developing novel opto-electronic applications. In general, synthesis of any kind of phosphor materials using the conventional/sol-gel technique would require laborious conditions such as hefty manual grinding, annealing, or calcination of samples to high temperature, intermediate grinding process, and heat treatment for several times, etc. In order to avoid the above mentioned difficulties, hydrothermal technique is the alternative and most promising approach to synthesize the variety of phosphor materials with desired size, shape, and dimensions, crystallinity by changing the experimental parameters.

Herein, we report the controlled synthesis of $(\text{Fe}_{0.5}\text{Gd}_{0.5})\text{MoO}_4:\text{Eu}^{3+}$ microcrystals (self-aggregated 3D superstructures) using hydrothermal method by employing PVP as the surfactant. By varying the reaction time, we have reported the morphology selection and the condition to derive novel nanoparticle sheathed bipyramid-like morphology. The rest of the parameters like molar ratio between initial precursor / surfactant and temperature were kept as constant. The $(\text{Fe}_{0.5}\text{Gd}_{0.5})\text{MoO}_4:\text{Eu}^{3+}$ microcrystals are found to be excellent matrix for photoluminescence property and the Eu^{3+} ion serves as a good red-emitting luminescent center. Further, room-temperature (RT) magnetic properties of $\text{Fe}_{0.5}\text{Gd}_{0.5}(\text{MoO}_4)_{1.5}:\text{Eu}^{3+}$ were investigated in detail.

3. Synthesis, morphology, structure of the $\text{Fe}_{0.5}\text{Gd}_{0.5}(\text{MoO}_4)_{1.5}:\text{Eu}^{3+}$ 3D hierarchical microstructures

3.1. Synthesis procedure

All the chemicals were purchased from Sigma Aldrich with 99.99% purity. In the typical synthesis, a stoichiometric amount of $\text{FeCl}_3 \cdot 6\text{H}_2\text{O}$ was dissolved in 15 mL of double-distilled water through vigorous stirring. Then, the appropriate amount of Na_2MoO_4 was initially dissolved in 30 mL of double-distilled water under vigorous stirring. Then, GdCl_3 and EuCl_3 were prepared by dissolving the corresponding rare-earth sesquioxides (Gd_2O_3 , Eu_2O_3) in diluted hydrochloric acid and stirred for 15 min. In order to remove the excess of HCl, the solution was heated to 60–80°C for 30 min. Then, the rare-earth chloride solution was carefully mixed into the Na_2MoO_4 solution. A white colloidal precipitate was obtained under vigorous stirring for 15 min. Subsequently, iron chloride solution was gradually introduced into the above white precipitate solution, forming a brown mixture solution. Then, 0.1 mM of polyvinylpyrrolidone (PVP40) was dissolved in 20 mL of double-distilled water, and was added to the resultant colloidal solution. Then, the pH value of the final product was consequently, adjusted to a value of 7–8 by adding the proper amount of sodium hydroxide solution. After additional stirring for 30 min, the acquired brown mixture solution was transferred into a 100 mL Teflon-lined stainless steel autoclave, and heated at 200°C for 6, 12, and 24 h. Finally, the autoclave was allowed to cool at room temperature, and the final product was centrifugally

cleaned (5,000 rpm for 30 min to remove organic containments and NaCl), separated from the solution, rinsed with distilled water and absolute ethanol several times, and dried at 60°C in the air for 5 h.

3.2. Characterization

XRD pattern of as-synthesized phosphor was analyzed using PANalytical's X'Pert PRO materials research, X-ray diffractometer equipped with a $\text{Cu-K}\alpha$ radiation ($\lambda = 1.54060 \text{ \AA}$) at a scanning rate of $0.02^\circ \text{ s}^{-1}$ performed in the range of 20–60 degrees. Morphology and energy-dispersive X-ray spectra (EDX) of the product were investigated by scanning electron microscope (FESEM (Quanta 3D FEG)). The spacing between the two adjacent lattice planes was measured using high-resolution transmission electron microscope (HRTEM JEOL 3010). Furthermore, the room-temperature (RT) photoluminescence studies were carried out using Horiba-Jobin Yvon Fluoramax-4P bench-top Spectrofluorometer. Room-temperature magnetic properties of the samples were analyzed using (Lake Shore 7307 model) vibrating sample magnetometer (VSM).

3.3. Morphological investigations

To explore the 3D surface morphology, particle size distribution, and formation mechanism for the evolution of nanoparticle sheathed bipyramid-like structures, a series of time-dependent experiments were carried out using a PVP employed hydrothermal route.

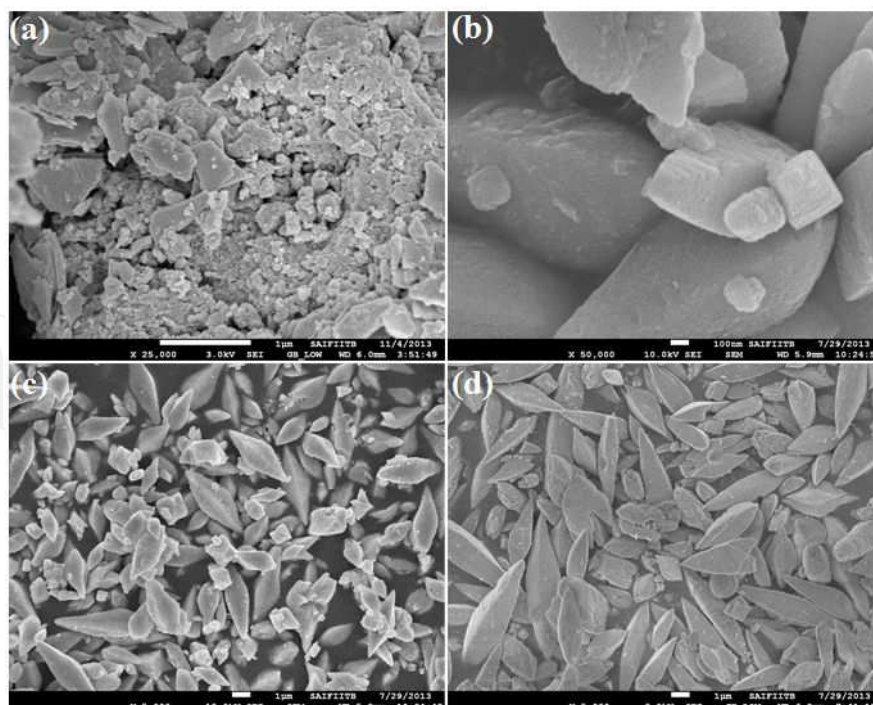


Figure 1. Field emission scanning electron microscopic images of $\text{Fe}_{0.5}\text{Gd}_{0.5}(\text{MoO}_4)_{1.5}:\text{Eu}^{3+}$ synthesized by PVP employed hydrothermal method with different time intervals, i.e., (a) 1 h, (b) 2 h, (c) 6 h, (d) 12 h at 200°C with fixed pH (~7).

The FESEM and TEM analyses were used to characterize the morphology of the final products. By changing the experimental reaction time interval with fixed temperature (200°C), pH (~7), and molar concentration of the PVP (0.1 mM), a substantial difference was observed in the final product. Figure (1–3) shows the low, high magnifications FESEM image of the $\text{Fe}_{0.5}\text{Gd}_{0.5}(\text{MoO}_4)_{1.5}:\text{Eu}^{3+}$ samples synthesized by hydrothermal route at different time intervals (1, 3, 6, 12, 24, and 48 h) with fixed temperature (200°C), pH (~7), and PVP molar concentration. During the initial period of 1 h time interval, numerous 2D nanoflakes with few tens of nanometer were observed, which acts as a primary building block for the subsequent growth of 3D microstructures (Figure 1 (a)). It was noticed from Figure 1 (b, c), when the hydrothermal time period was increased to 3 and 6 h, nanoflakes began to self-organize continuously through plane-to-plane coalition and try to form a bipyramidal morphology (average diameter of 1 μm). However, the morphology and size distribution was found to be less uniform. When the reaction time interval was kept at 12 h, bipyramid-like morphology with an average of 1.0 μm in length and an average of 1.2 μm in diameter was obtained and shown in Fig. 1 (d). When the reaction time period was raised to 24 h, highly ordered and self-assembled porous nanoparticle sheathed bipyramid-like morphology with the size approximately equal to ~1.2 μm diameter was observed (Figure 2 (a, b)). Further, increasing the reaction time to 48 h, the final product morphology consisted of irregular porous bipyramid-like structures in which nanoparticles are sheathed and shown in Figure 2 (c, d). This may be due to the prolonged time interval, resulting in thermal collision between the particles (growth stage; the self-assembly process predominates between these crystals because of its high surface energies) [14].

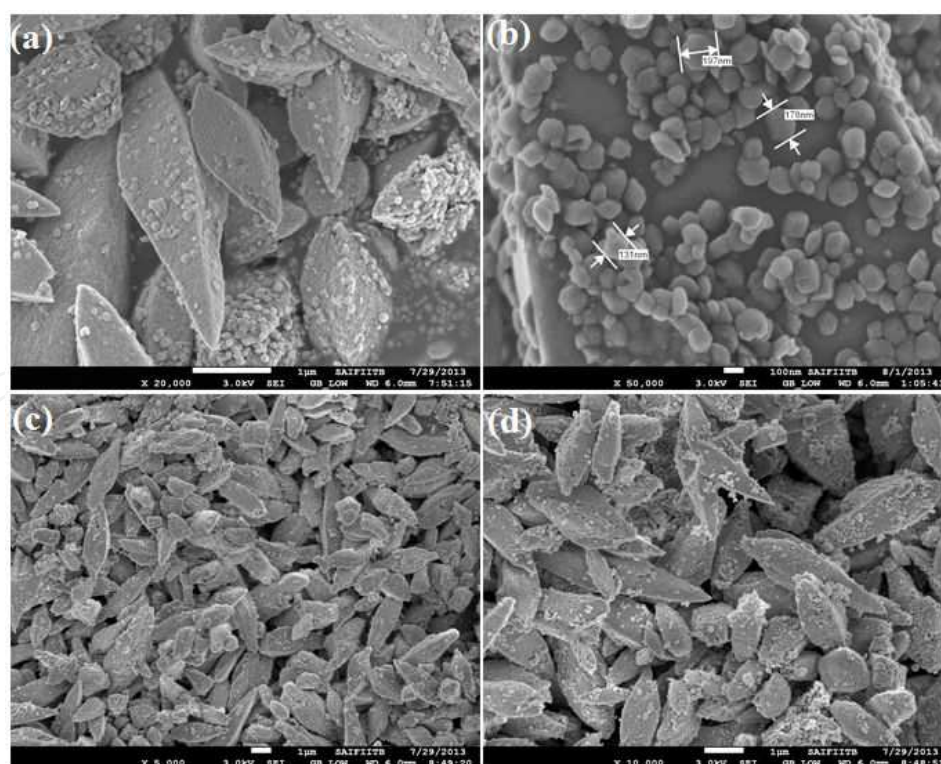


Figure 2. Low and high magnification SEM images of self-assembled nanoparticle sheathed $\text{Fe}_0\text{Gd}_{0.5}(\text{MoO}_4)_{1.5}:\text{Eu}^{3+}$ structures synthesized at (a, b) 24 and (c, d) 48 h.

This involves growth from 0D primary particles to 2D nanosheets, followed by the formation of 3D hierarchical networks through an assembly–disassembly process [14]. The TEM image of the sample synthesized at 24 h time interval with 0.1 mM of PVP molar concentration is shown in Figure 3a and the corresponding inset shows the FFT pattern. The formation mechanism for the evolution of a nanoparticle-sheathed bipyramid-like $\text{Fe}_{0.5}\text{Gd}_{0.5}(\text{MoO}_4)_{1.5}:\text{Eu}^{3+}$ structure can be described as follows. Primarily, smaller crystalline nuclei formed in a supersaturated solution starts the crystallization process for subsequent growth of self-organization. During the self-organization process, smaller nanocrystals were grown-up constantly to form bigger particles via an Ostwald ripening phenomenon at higher reaction time intervals, due to interactions between the amorphous nanoparticles, resulting in 2D nanoflakes [14]. Initially, PVP acts as a surface capping agent to form a stable complex with $\text{Gd}^{3+}/\text{Fe}^{3+}$ and then kinetically controls the reaction rate, germination of nuclei, the growth rate, and the oriented aggregation mechanism. When the reaction temperature gradually increases to higher temperature, PVP would decompose gradually and has no obvious effect on the possible growth of nuclei. When the time period was increased, these 2D nanoflakes joined each other along a mutual crystallographic orientation through plane-to-plane conjunction of neighboring particles [14]. In general, such amalgamation process between the atoms/ions in molecules/crystals can induce dipole moments, which can be associated with certain specific crystallographic orientations [13]. The interaction among dipole moments in nearby nanoparticles is highly probable and acts as a driving factor for the oriented attachment procedure by allocation of a common crystallographic facet. The growth rate in $\text{Fe}_0\text{Gd}_{0.5}(\text{MoO}_4)_{1.5}:\text{Eu}^{3+}$ crystals is oriented preferentially along the [001] direction. Donnay-Harker et al. [5] reported that, for tetragonal structures, the surface free energy of the [001] face is larger than that of the [101] face [5, 2]. As a result, the faster growth rate in the [100], [010], and [001] faces in comparison with that in the [101] direction accelerates the formation of self-assembled structures.

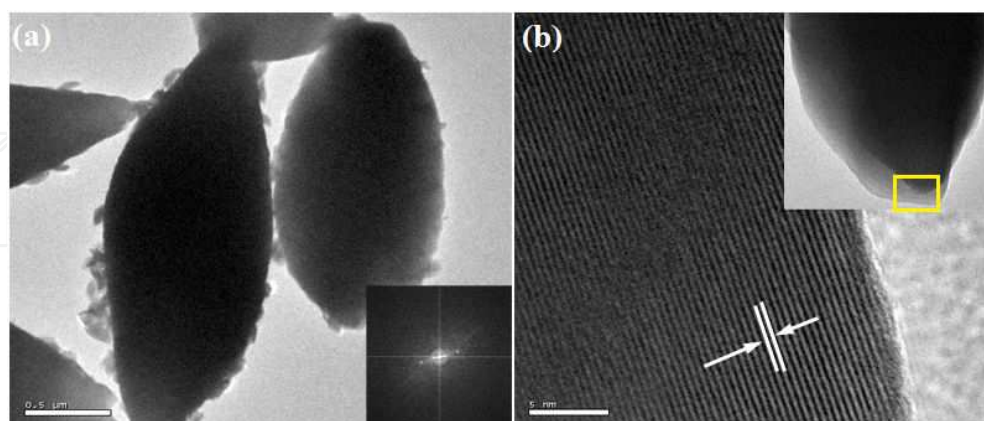


Figure 3. (a) TEM image of the $\text{Fe}_{0.5}\text{Gd}_{0.5}(\text{MoO}_4)_{1.5}:\text{Eu}^{3+}$ sample prepared at 24 h time interval and the corresponding inset shows the FFT pattern, (b) HRTEM image (inset typical HRTEM image taken on the marked part).

The as-grown 2D nanoflakes are continuously self-assembled via a layer-by-layer stacking process to form 3D bipyramid-like structures. Then, the completely developed bipyramid

particles are readily disassembled into smaller nanoparticles, which are finally sheathed on individual bipyramid-like particles. After aging for a longer time period, the disassembly of well-organized structures could increase the entropy of the system and thus could decrease the free energy of the whole system [16], resulting in the nanoparticles arbitrarily sheathed on individual bipyramid-like particles. The assembly–disassembly process in $\text{Fe}_0\text{Gd}_{0.5}(\text{MoO}_4)_{1.5}:\text{Eu}^{3+}$ was described in our previous work [13] by using EDTA as a surface capping agent.

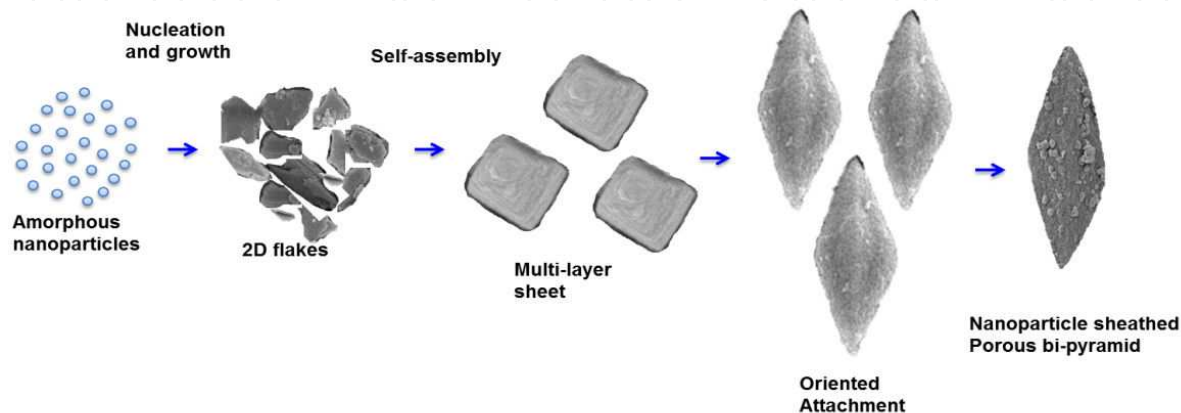


Figure 4. Schematic diagram illustrating the formation mechanism of nanoparticle sheathed $\text{Fe}_0\text{Gd}_{0.5}(\text{MoO}_4)_{1.5}:\text{Eu}^{3+}$ 3D hierarchical structures.

3.4. Structural analysis

The chemical phase purity and crystalline nature of the product were investigated using X-ray diffraction patterns. Figure 5 shows the XRD pattern of $\text{Fe}_{0.5}\text{Gd}_{0.5}(\text{MoO}_4)_{1.5}:\text{Eu}^{3+}$ samples synthesized by a facile hydrothermal route at different time intervals (6, 12, 24, and 48 h). All the peaks are perfectly matched with the standard JCPDS card no. 25-0828 of $(\text{Na}_{0.5}\text{Gd}_{0.5})\text{MoO}_4$. It could be clearly observed that the XRD patterns of as-synthesized samples are highly crystalline, and the strongest intensity peak is observed at $2\theta = 28.67$ degrees analogous to (112) plane. The XRD pattern reveals that they belong to a tetragonal phase corresponding to the scheelite structure with the space group $I4_1/a$. In this crystal structure Fe^{3+} , $\text{Gd}^{3+}/\text{Eu}^{3+}$ ions jointly occupy the dodecahedral sites of the tetrahedra. Molybdenum atoms (Mo^{6+}) populated in the center of tetrahedral symmetry is surrounded by four equivalent oxygen (O^{2-}) atoms [13] and forming isolated $[\text{MoO}_4]^{2-}$ group. Owing to their similar ionic radius and valance state, the Eu^{3+} ion successfully replaces the Gd^{3+} ion and does not change the lattice site of the host $\text{Fe}_{0.5}\text{Gd}_{0.5}(\text{MoO}_4)_{1.5}:\text{Eu}^{3+}$ and the crystal phase is very much pure. Further, no other extra peaks of impurity were observed.

Figure 5 (a, b) shows the representative EDX analysis, taking single bipyramid-like particle and single nanoparticle sheathed on bipyramidal structure synthesized at 24 h time interval for Eu^{3+} doped $\text{Fe}_{0.5}\text{Gd}_{0.5}(\text{MoO}_4)_{1.5}$. The energy-dispersive X-ray spectrum was used to confirm the presence of iron (Fe^{3+}), gadolinium (Gd^{3+}), europium (Eu^{3+}), molybdenum (Mo^{6+}), and

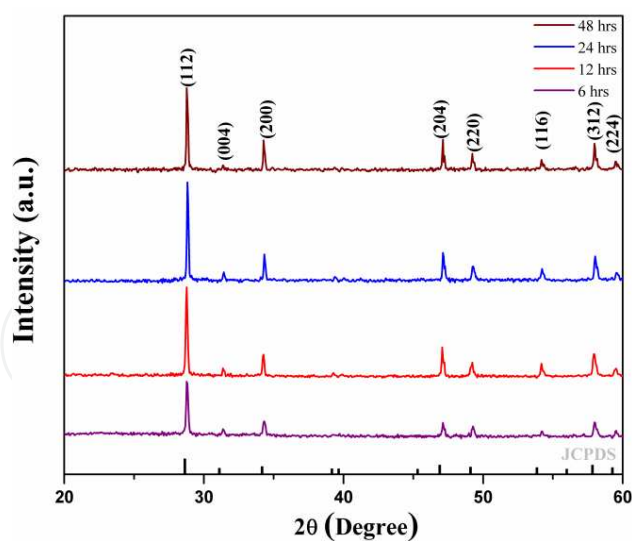


Figure 5. Powder X-ray diffraction (XRD) patterns of the $\text{Fe}_{0.5}\text{Gd}_{0.5}(\text{MoO}_4)_{1.5}:\text{Eu}^{3+}$ samples synthesized at different time intervals using the PVP-mediated hydrothermal method.

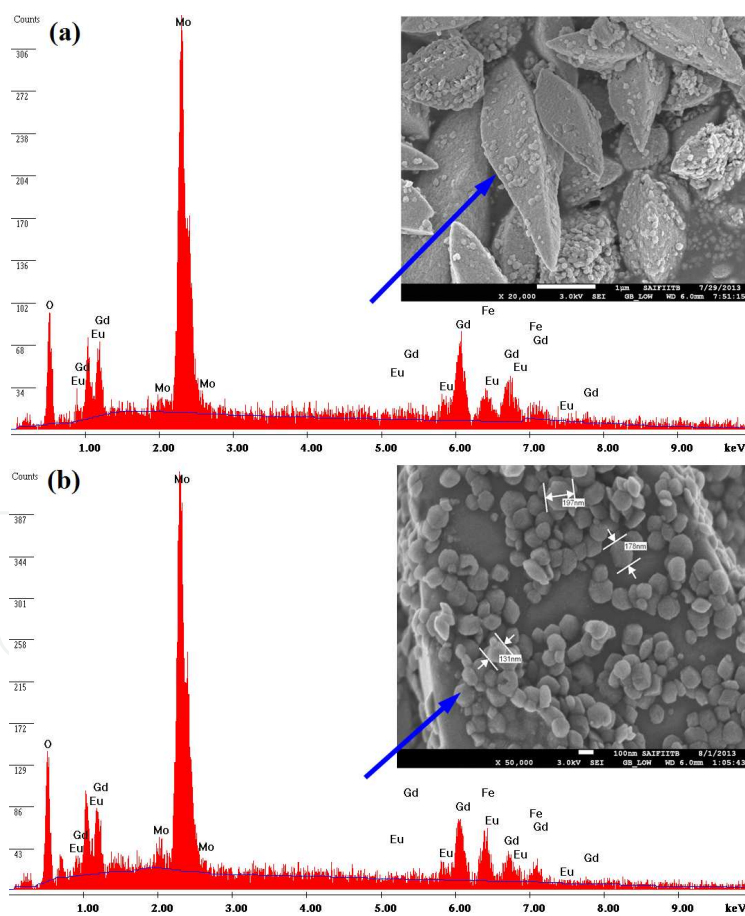


Figure 6. (a) EDX spectrum of single bipyramid-like $\text{Fe}_{0.5}\text{Gd}_{0.5}(\text{MoO}_4)_{1.5}:\text{Eu}^{3+}$ particle, (b) EDX spectrum of single nanoparticle sheathed on a bipyramid-like particle.

oxygen (O^{2-}) in the final product. The EDX spectrum shown in Figure 5 (a, b) confirms the presence of Fe, Gd, Eu, Mo, and O in the final product.

3.5. Optical and magnetic properties of $Fe_{0.5}Gd_{0.5}(MoO_4)_{1.5}:Eu^{3+}$ structures

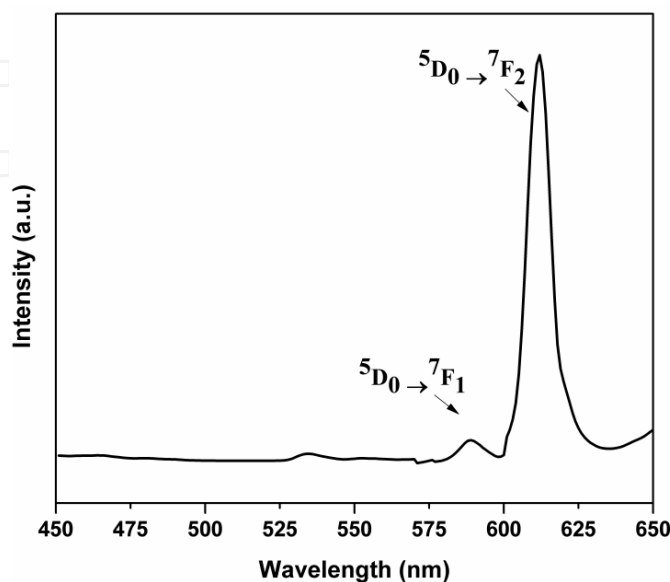


Figure 7. Room temperature emission spectra of Eu^{3+} doped $Fe_{0.5}Gd_{0.5}(MoO_4)_{1.5}$ synthesized by the PVP-assisted hydrothermal route.

Figure 7 shows the PL excitation and emission spectra of nanoparticle sheathed bipyramid-like microstructures of $Fe_{0.5}Gd_{0.5}(MoO_4)_{1.5}:Eu^{3+}$. Emission ($\lambda_{ex} = 395$ nm) spectra of the $Fe_{0.5}Gd_{0.5}(MoO_4)_{1.5}$ doped with Eu^{3+} ions were recorded within the range from 575 to 700 nm at room temperature. Upon 395 nm UV irradiation, the emission spectrum was governed by the hypersensitive red emission, showing a transition $^5D_0 \rightarrow ^7F_2$ (due to electric dipole transition) higher than $^5D_0 \rightarrow ^7F_1$ (magnetic dipole). In the emission spectrum, the transitions $^5D_0 \rightarrow ^7F_J$ (where $J = 1, 2, 3, 4$) were observed due to intra-configurational f–f electronic transitions of Eu^{3+} ions. The presence of electric dipole transition confirmed that Eu^{3+} ions were located at sites without inversion symmetry (C_{3v} symmetry). The other transitions $^5D_0 \rightarrow ^7F_3$ and $^5D_0 \rightarrow ^7F_4$ were comparatively very weak for all the samples (not shown in PL spectrum). However, the presence of magnetic iron (Fe^{3+}) in the $Fe_{0.5}Gd_{0.5}(MoO_4)_{1.5}$ tetragonal crystal structure considerably decreases their luminescence, as Fe^{3+} ions share the dodecahedral sites with Gd^{3+}/Eu^{3+} [13]. However, it is still unclear for the weak red emission in Eu^{3+} doped $Fe_{0.5}Gd_{0.5}(MoO_4)_{1.5}$.

Figure 8 shows the room-temperature (RT) magnetic properties of hierarchically self-organized $Fe_{0.5}Gd_{0.5}(MoO_4)_{1.5}:Eu^{3+}$ 3D microstructures synthesized by the hydrothermal route at 24 h time interval. Magnetization as a function of applied magnetic field (from 15000 Oe to 15000 Oe) was measured using a vibrating sample magnetometer. Due to the presence of Gd^{3+} ions, a magnetic hysteresis (M–H) loop was not observed in the case of Eu^{3+} doped $Fe_{0.5}Gd_{0.5}(MoO_4)_{1.5}$. From Figure 8, it is clear that a straight line crosses the origin, indicating that the phosphor $Fe_{0.5}Gd_{0.5}(MoO_4)_{1.5}:Eu^{3+}$ exhibits a paramagnetic behavior due to the existence

of paramagnetic Gd^{3+} ions and the saturation magnetization (M_s) value is found to be 0.028 emu/gm for RT. The extremely localized nature of the seven unpaired inner 4f electrons of Gd plays an important role which determines its magnetic properties [15]. These unpaired electrons in the outer orbital are closely bound to the nucleus and effectively shielded by the outer closed shell electrons $5s^2 5p^6$ from the crystal field [15]. Even though the Gd^{3+} ions jointly occupy the dodecahedral sites with Fe^{3+} ions, number of 4f electrons in the Gd^{3+} ions, atomic unit cell volume, direct f–f exchange interactions between neighboring Gd^{3+} and Fe^{3+} atoms are responsible for setting up the magnetic moments [15, 14]. Since, Gd^{3+} ions have total orbital angular momentum $L = 0$ [13], the spin orbit coupling between the partially filled 4f electrons in the Gd^{3+} and Fe^{3+} ions is weak, which inhibits sufficient orbital overlaps [8].

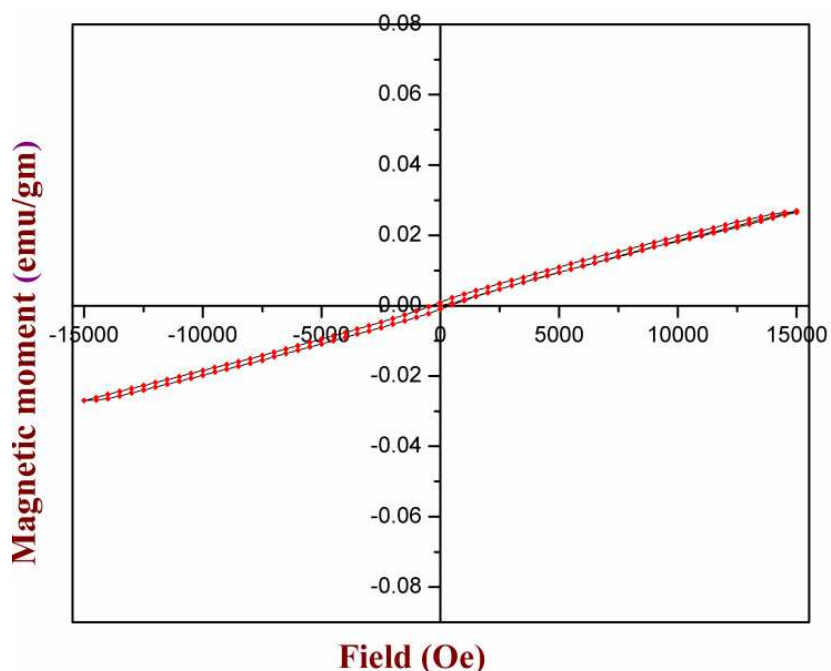


Figure 8. Magnetization vs. magnetic field of the as-synthesized bipyramid-like structures of $\text{Fe}_{0.5}\text{Gd}_{0.5}(\text{MoO}_4)_{1.5}:\text{Eu}^{3+}$ synthesized by hydrothermal treatment at 200°C for 24 h.

4. Conclusion

In summary, the interaction between the Gd^{3+} and Fe^{3+} ions in the crystal structure $\text{Fe}_{0.5}\text{Gd}_{0.5}(\text{MoO}_4)_{1.5}:\text{Eu}^{3+}$ is weak and hence insufficient overlap of the orbitals associated with 4f shells gives rise to paramagnetism. Further, more detailed investigations are required to determine the magnetic behavior of $\text{Fe}_{0.5}\text{Gd}_{0.5}(\text{MoO}_4)_{1.5}:\text{Eu}^{3+}$ at various temperatures. The nanoparticle sheathed $\text{Fe}_{0.5}\text{Gd}_{0.5}(\text{MoO}_4)_{1.5}:\text{Eu}^{3+}$ porous bipyramid-like structures were successfully synthesized using hydrothermal technique by employing PVP as the surfactant. The hydrothermal reaction time period was the key parameter and plays an important role for morphological evolution of self-aggregated 3D hierarchical networks. A possible growth

mechanism for the formation of microstructures clearly involves the layer-by-layer self-assembly of 2D nanoflakes with successive disassembly, via an Ostwald ripening phenomena. The photoluminescence emission properties of Eu^{3+} doped $\text{Fe}_{0.5}\text{Gd}_{0.5}(\text{MoO}_4)_{1.5}$ were investigated. Under the excitation of 395 nm UV light, the as-synthesized samples show red emission from the hypersensitive ${}^5\text{D}_0 \rightarrow {}^7\text{F}_2$ transition at 615 nm. RT magnetic properties of the nanoparticles sheathed porous bipyramid-like $\text{Fe}_{0.5}\text{Gd}_{0.5}(\text{MoO}_4)_{1.5}:\text{Eu}^{3+}$ structures clearly exhibit the paramagnetic behavior due to the presence of paramagnetic Gd^{3+} ions. The current experimental results are important and may open up a new scope for the design and formulation of bifunctional magnetic and luminescence applications.

Author details

Rajagopalan Krishnan¹ and Jagannathan Thirumalai^{2*}

*Address all correspondence to: thirumalaijg@gmail.com

1 Department of Physics, Rajalakshmi Institute of Technology, Kuthampakkam, Chennai, Tamil Nadu, India

2 Department of Physics, B. S. Abdur Rahman University, Vandalur, Chennai, Tamil Nadu, India

References

- [1] Ajithkumar G, Yoo B, Goral DE, Hornsby PJ, Lin A-L, Ladiwala U, Dravid VP, & Sardar DK. Multimodal bioimaging using a rare earth doped $\text{Gd}_2\text{O}_3:\text{Yb}/\text{Er}$ phosphor with upconversion luminescence and magnetic resonance properties. *J Mater Chem B* 2013;1(11):1561–72 (January 2013), ISSN: 2050–750X.
- [2] Bu W, Chen Z, Chen F, Shi J. Oleic acid/oleylamine cooperative-controlled crystallization mechanism for monodisperse tetragonal bipyramid $\text{NaLa}(\text{MoO}_4)_2$ Nanocrystals. *J Phys Chem C* 2009;113(28):12176–85 (June 2009), ISSN: 1932–7447.
- [3] Cavalcante L.S, Almeida MAP, Avansi W, Tranquilin RL, Longo E, Batista NC, Mastelaro VR, Li MS. Cluster coordination and photoluminescence properties of $\alpha\text{-Ag}_2\text{WO}_4$ microcrystals. *Inorg Chem* 2012a;51:10675–87 (September 2012), ISSN: 0020-1669.
- [4] Cavalcante LS, Longo VM, Sczancoski JC, Almeida MAP, Batista AA, Varela JA, Orlandi MO, Longo E, Li MS. Electronic structure, growth mechanism and photoluminescence of CaWO_4 crystals. *Cryst Eng Comm* 2012b;14:853–68 (November 2012), ISSN: 1466-8033.

- [5] Donnay JDH, Harker D. A new law of crystal morphology extending the law of Bravais. *Am Mineral* 1937;22(5):446–47 (May 1937), ISSN: 0003-004x.
- [6] Gupta BK, Narayanan TN, Vithayathil SA, Lee Y, Koshy S, Reddy ALM, Saha A, Shanker V, Singh VN, Kaiparettu BA, Martí AA, Ajayan PM. Highly luminescent-paramagnetic nanophosphor probes for in vitro high-contrast imaging of human breast cancer cells. *Small* 2012;19(8):3028–34 (October 2012), ISSN: 1613-6829.
- [7] Han L, Xiaohong Y, Xiangfu W. Controllable synthesis and down-conversion properties of flower-like $\text{NaY}(\text{MoO}_4)_2$ microcrystals via polyvinylpyrrolidone-mediated. *J Solid State Chem* 2013;204:266–71 (June 2013), ISSN: 0022-4596.
- [8] He F, Niu N, Wang L, Xu J, Wang Y, Yang G, Gai S Yang P. Influence of surfactants on the morphology, upconversion emission, and magnetic properties of β - $\text{NaGdF}_4:\text{Yb}^{3+}, \text{Ln}^{3+}$ (Ln = Er, Tm, Ho). *Dalton Trans* 2013;42:(27)10019–28 (April 2013), ISSN: 1477-9226.
- [9] Huang S, Zhang X, Wang L, Bai L, Xu J, Li C, Yang P. Controllable synthesis and tunable luminescence properties of $\text{Y}_2(\text{WO}_4)_3:\text{Ln}^{3+}$ (Ln = Eu, Yb/Er, Yb/Tm and Yb/Ho) 3D hierarchical architectures. *Dalton Trans* 2012;41(18):5634–42 (February 2012), ISSN: 1477-9226.
- [10] Jayanthi K, Manorama, SV. Lumino-magnetic YAG:Ce nanophosphors: novel synthesis routes for efficient luminescence and magnetic properties. *J Mater Chem C* 2014;2(48):10322–30 (October 2014), ISSN: 2050-7526.
- [11] Kaczmareka AM, Deun RV. Rare earth tungstate and molybdate compounds from 0D to 3D architectures. *Chem Soc Rev* 2013;42(23):8835–48 (September 2013), ISSN: 0306-0012.
- [12] Krishnan R, Thirumalai J, Banu IBS, Chandramohan R. Influence of Eu^{3+} ions in $\text{Na}_{0.5}\text{La}_{0.5}\text{MoO}_4$: structural and optical investigation. *J Mater Sci: Mater Electron* 2013;24:(12):4774–81 (September 2013), ISSN: 0957-4522.
- [13] Krishnan R, Thirumalai J, Kathiravan A. Luminescence and magnetic properties of novel nanoparticle-sheathed 3D micro-architectures of $\text{Fe}_{0.5}\text{R}_{0.5}(\text{MoO}_4)_{1.5}:\text{Ln}^{3+}$ (R = $\text{Gd}^{3+}, \text{La}^{3+}$), (Ln = Eu, Tb, Dy) for bi-functional application. *Elect Mat Let* 2015;11(1): 24–33 (January 2015) ISSN: 1738-8090.
- [14] Krishnan R, Thirumalai J, Thomas S, Gowri M. Luminescence and magnetic behaviour of almond like $(\text{Na}_{0.5}\text{La}_{0.5})\text{MoO}_4:\text{RE}^{3+}$ (RE = Eu, Tb, Dy) nanostructures. *J Alloys Compd* 2014b;604:20–30 (March 2014), ISSN: 0925-8388.
- [15] Krishnan R, Thirumalai J. Up/down conversion luminescence properties of $(\text{Na}_{0.5}\text{Gd}_{0.5})\text{MoO}_4:\text{Ln}^{3+}$ (Ln = Eu, Tb, Dy, Yb/Er, Yb/Tm, and Yb/Ho) microstructures: synthesis, morphology, structural and magnetic investigation. *New J Chem* 2013a; 38(8):3480–91 (May 2014), ISSN: 1144-0546.

- [16] Li G, Li L, Li M, Bao W, Song Y, Gan S, Zou H, Xu X. Hydrothermal synthesis and luminescent properties of $\text{NaLa}(\text{MoO}_4)_2:\text{Eu}^{3+}, \text{Tb}^{3+}$ phosphors. *J Alloys Compd* 2013a; 550:1–8 (February 2013), ISSN: 0925-8388.
- [17] Li Z, Li C, Mei Y, Wang L, Du G, Xiong Y. Synthesis of rhombic hierarchical YF_3 nanocrystals and their use as upconversion photocatalysts after TiO_2 coating. *Nanoscale* 2013b;5(7):3030–36 (February 2013), ISSN: 2040-3364.
- [18] Liu X, Li L, Noh HM, Jeong JH, Jang H, Shin DS. Controllable synthesis of uniform $\text{CaMoO}_4:\text{Eu}^{3+}, \text{M}^+$ ($\text{M} = \text{Li}, \text{Na}, \text{K}$) microspheres and optimum luminescence properties. *RSC Adv* 2015;5(13):9441–54 (January 2015), ISSN: 2046-2069.
- [19] Ma ZY, Dosev D, Nichkova M, Gee SJ, Hammock BD, Kennedy IM. Synthesis and bio-functionalization of multifunctional magnetic $\text{Fe}_3\text{O}_4@Y_2\text{O}_3:\text{Eu}$ nanocomposites. *J Mater Chem* 2009;19(27):4695–700 (May 2009) ISSN: 0959-9428.
- [20] Mahalingam V, Thirumalai J, Krishnan R, Chandramohan R. Potential visible light emitting rare-earth activated $\text{Ca}_{0.5}\text{Y}_{1-x}(\text{MoO}_4)_2:x\text{RE}^{3+}$ ($\text{RE} = \text{Pr}, \text{Sm}, \text{Eu}, \text{Tb}, \text{Dy}$) phosphors for solid state lighting applications. *J Mater Sci: Mater Electron* 2014;26(2):842–52 (November 2014), ISSN: 0957-4522.
- [21] Park SW, Moon BK, Choi BC, Jeong JH, Bae JS, Kim KH. Red photoluminescence of pulsed laser deposited $\text{Eu}:\text{NaY}(\text{MoO}_4)_2$ thin film phosphors on sapphire substrates. *Curr Appl Phys* 2012;12(2):S150–5 (February 2012), ISSN: 1567-1739.
- [22] Shi J, Liu D, Tong L, Yang X, Yang H. Magnetic and photoluminescence properties of $\text{Fe}_3\text{O}_4@\text{SiO}_2@Y\text{P}_{1-x}\text{V}_x\text{O}_4:\text{Dy}^{3+}$ nanocomposites. *J Alloys Compd* 2011;509(42):10211-16 (October 2011), ISSN: 0925-8388.
- [23] Thirumalai J, Chandramohan R, Basheer Ahamed M, Ezhilvizhian S, Vijayan TA. Pr^{3+} doped BaMoO_4 octahedron to shuttle-like microcrystals: synthesis and luminescence properties. *J Mater Sci: Mater Electron* 2012;23(1):325–33 (May 2012), ISSN: 0957-4522.
- [24] Thirumalai J, Krishnan R, Banu IBS, Chandramohan R. Controlled synthesis, formation mechanism and luminescence properties of novel 3-dimensional $\text{Gd}_2(\text{MoO}_4)_3:\text{Eu}^{3+}$ nanostructures. *J Mater Sci: Mater Electron* 2013;24(1):253–59 (January 2013), ISSN: 0957-4522.
- [25] Wang W, Zou M, Chen K. Novel $\text{Fe}_3\text{O}_4@Y\text{PO}_4:\text{Re}$ ($\text{Re} = \text{Tb}, \text{Eu}$) multifunctional magnetic–fluorescent hybrid spheres for biomedical applications. *Chem Commun* 2010;46(28):5100–102 (May 2010) ISSN: 1359-7345.
- [26] Xu L, Yang X, Zhai Z, Chao X, Zhang Z, Hou W. EDTA-mediated hydrothermal synthesis of $\text{NaEu}(\text{MoO}_4)_2$ microrugbies with tunable size and enhanced luminescence properties. *Cryst Eng Comm* 2011;13(15):4921–29 (June 2011), ISSN: 1466-8033.
- [27] Xu L, Yang X, Zhai Z, Gu D, Pang H, Hou W. Self-assembled 3D architectures of $\text{NaCe}(\text{MoO}_4)_2$ and their application as absorbents. *Cryst Eng Comm* 2012;14(21):7330–37 (August 2012), ISSN: 1466-8033.

- [28] Yan B, Wu J. Facile composite synthesis and photoluminescence of $\text{NaGd}(\text{MoO}_4)_2:\text{Ln}^{3+}$ ($\text{Ln} = \text{Eu}, \text{Tb}$) submicrometer phosphors. *J Mater Res* 2011;24(1):32–38 (January 2011), ISSN: 0884-2914.
- [29] Zhang L, Cao XF, Ma Y-L, Chen X-T, Xue Z-L. Pancake-like $\text{Fe}_2(\text{MoO}_4)_3$ microstructures: microwave-assisted hydrothermal synthesis, magnetic and photocatalytic properties. *New J Chem* 2010;34(9):2027–33 (May 2010), ISSN: 1144-0546.
- [30] Zhang Y, Zheng A, Yang X, He H, Fan Y, Yao C. Cubic GdFeO_3 particle by a simple hydrothermal synthesis route and its photoluminescence and magnetic properties. *Cryst Eng Comm* 2012;14(24):8432–39 (September 2012), ISSN: 1466-8033.

